Solid State Nuclear Magnetic Resonance **22**, 97–109 (2002)
doi:10.1006/snmr.2002.0084

Investigations of Low-Amplitude Radio Frequency Pulses at and away from Rotary Resonance Conditions for $I = \frac{5}{2}$ Nuclei[1]

John W. Logan, Jeffry T. Urban, Jamie D. Walls, Kwang Hun Lim, Alexej Jerschow,[2] and Alexander Pines[3]

Materials Sciences Division, 1 Cyclotron Rd, Lawrence Berkeley National Laboratory, Berkeley, California 94720; and Department of Chemistry, University of California at Berkeley, Berkeley, California 94720

FESTSCHRIFT IN HONOR OF PROFESSOR HANS-WOLFGANG SPIESS ON THE OCCASION OF HIS 60TH BIRTHDAY

Additional experimental evidence of rotary resonance effects for multiple-quantum coherence conversion in a spin-5/2 system is presented. Two-dimensional plots of the relative efficiency of MQ excitation and conversion are given as a function of radio frequency (rf) amplitude and pulse width. Data are presented for the excitation of five-quantum coherence (5QC), as well as for 5QC to three-quantum coherence (3QC) conversion, 5QC to 1QC (the central transition coherence) conversion, and 3QC to 1QC conversion. A two-fold increase in the signal-to-noise ratio is achieved by substituting low amplitude rf pulses in place of hard rf pulses for 5QC excitation and 5QC to 3QC conversion in a mixed multiple-quantum magic angle spinning (MAS) (MMQMAS) experiment. The anisotropic line shape for the low-amplitude rf pulse version of the MMQMAS experiment was observed to be distorted from the MAS line shape. The cause and implications of the distortion are discussed.

Key Words: quadrupolar NMR; MQMAS; mixed multiple-quantum MAS; rotary resonance; sensitivity enhancement; orientation selective pulses.

INTRODUCTION

Quadrupolar nuclei (i.e. those with a nuclear spin $I > \frac{1}{2}$) are present in a wide variety of solid materials, including glasses, minerals, zeolites, catalysts, inorganic compounds, and biomolecules. Quadrupolar nuclei have a non-spherical charge distribution that interacts with the electric field gradient (EFG) due to the local electronic environment of the nucleus [1]. Knowledge of the EFG can be used to help elucidate structural characteristics, such as the coordination numbers and the geometry of neighboring atoms [2–5]. Static NMR spectra of multiple resonances are difficult, if not impossible, to interpret since the quadrupolar broadening is large compared to the chemical shift range, resulting in overlapping resonances. Accurate

[1]Presented, in part, at the 2nd Alpine Conference on Solid-State NMR, France, 9–13 September 2001.
[2]Present address: New York University, Chemistry Department, New York, New York 10003.
[3]To whom correspondence should be addressed. Materials Sciences Division, 1 Cyclotron Rd, Lawrence Berkeley National Laboratory, Berkeley, California 94720. Fax: 510-486-5744. E-mail: pines@cchem.berkeley.edu.

0926-2040/02 $35.00

structural information plays a major role in the understanding of the functionality and physical properties of the materials. Consequently, high-resolution techniques are generally required in order to extract useful information from the solid-state NMR spectra of materials.

Throughout the rest of this article, all coherences are assumed to be symmetric coherences ($|m\rangle \leftrightarrow |-m\rangle$). The effects of the first-order quadrupolar interaction can be neglected during periods of free evolution by considering only symmetric transitions. Magic angle spinning (MAS) averages away the anisotropic second-rank components of the second-order quadrupolar interaction; however, the remaining anisotropic fourth-rank components of the second-order quadrupolar interaction still broaden the resonances. In 1995, Frydman and coworkers introduced the multiple-quantum MAS (MQMAS) technique for removing the second-order quadrupolar broadening [6, 7]. A combination of symmetric multiple-quantum and single-quantum coherences is used in half-integer spins to remove the anisotropic fourth-rank terms of the second-order quadrupolar interaction. A two-dimensional data set is obtained that has an isotropic spectrum in the indirect dimension, F_1, and, in principle, the MAS spectrum along the direct dimension, F_2.

One aspect of the MQMAS experiment that has received much attention in recent years is the improvement of the radio frequency (rf) pulses that excite multiple-quantum coherences (MQCs) or convert MQCs to single-quantum coherence. The improved pulses are more efficient and therefore increase the sensitivity of the experiment [8–19]. Many of these techniques require rf pulses with large amplitudes in order to induce coherence transfer. However, recently Vosegaard *et al.* [17] discovered a new method (FASTER MQMAS) for increasing the sensitivity of the MQMAS experiment using low-amplitude rf pulses.

Rotary resonance (RR) effects are observed when the strength of the rf field matches a multiple of the rotor spinning speed. The FASTER MQMAS experiment on $I = 3/2$ nuclei was the first implementation of RR rf pulses in the MQMAS experiment [17]. Walls *et al.* [20] subsequently provided a bimodal Floquet treatment [21–23] to explain these results in spin $I = 3/2$ systems; predictions also were made for higher spins. Later, Gan and Grandinetti used a unimodal Floquet treatment to explain the RR effects in FASTER MQMAS [24]. The theory for $I = 5/2$ also has been presented by Walls *et al.* [25], again using a bimodal Floquet treatment.

RR effects are not limited to MQC excitation and conversion. RR pulses also have been used in spin-1/2 systems to probe chemical shift anisotropy and dipole–dipole interactions [26–29]. The RR effects in half-integer quadrupolar systems were described previously as anomalies in the spin locking efficiencies in the sudden-passage regime [30, 31], since they were not predicted by Vega's theory [32, 33] for spin locking the central transition (CT) of half-integer quadrupolar nuclei. Presently, the low-spin locking efficiency is believed to be caused by mixing of the CT coherence into MQCs at RR conditions.

In this article, we present 2D maps showing the efficiency of various coherence transfers in a spin $I = 5/2$ system as a function of rf amplitude and pulse width. RR effects are observed during MQC excitation and conversion. We demonstrate that an increase in sensitivity by a factor of two be obtained when using appropriately chosen low-amplitude rf pulses (LAPs) for the five-quantum coherence (5QC)

excitation and 5QC to three-quantum coherence (3QC) conversion in a 5Q3Q mixed multiple-quantum magic angle spinning (MMQMAS) experiment [34], when compared to the corresponding hard pulse version of the experiment. Although the sensitivity of the experiment is enhanced when low-amplitude rf pulses are substituted for hard rf pulses, the anisotropic line shape is distorted, since only a fraction of the crystallite orientations contributes to the signal.

THEORY

Removing the Second-Order Quadrupolar Broadening

Neglecting the effects of scalar and dipolar couplings, the frequency of a symmetric p-quantum transition ($|m = -p/2\rangle \leftrightarrow |m = +p/2\rangle$) of a quadrupolar spin with spin number I under MAS is given (to second order in perturbation theory) by

$$\omega(p, \alpha, \beta, \gamma) = \omega_0^{\mathrm{CS}} p + \omega_0^{Q} C_0^I(p) + \omega_4^{Q}(\alpha, \beta, \gamma) C_4^I(p) P_4(\cos\theta_m), \tag{1}$$

where ω_0^{CS} is the isotropic chemical shift (CS) frequency, ω_l^Q are the second-order quadrupolar frequencies of rank l, and $P_4(\cos\theta)$ is the fourth-rank Legendre polynomial. α, β and γ are Euler angles relating the frame of the EFG tensor in its principal axis system (PAS) to the rotor-fixed frame. θ_m is the angle between the B_0 field and the rotor axis (the magic angle), $\theta_m = \arctan(\sqrt{2})$. $\omega_0^{Q,\mathrm{CS}}$ are scalars and therefore do not depend on orientation. The coefficients $C_l^I(p)$ can be calculated using the following equations [7]:

$$C_0^I(p) = p[I(I+1) - \tfrac{3}{4}p^2], \tag{2}$$

$$C_4^I(p) = p[18I(I+1) - \tfrac{17}{2}p^2 - 5]. \tag{3}$$

(The anisotropic second-rank term in Eq. (1) is not included since it is zero under MAS.)

Consider an experiment with evolution under two different symmetric MQ coherence orders during t_1. Let the two coherence orders, p_1 and p_2, evolve for delays $\tau_1 = at_1$ and $\tau_2 = bt_1$, respectively, where a and b are positive and sum to unity. a and b are chosen to refocus the fourth-rank anisotropic quadrupolar interaction (and not to refocus the CS or the second-order quadrupolar isotropic shift). The anisotropic second-order quadrupolar interaction is removed at the end of t_1 if a and b satisfy [35]

$$C_4^I(p_1)a + C_4^I(p_2)b = 0, \tag{4}$$

resulting in an isotropic line shape in the F_1 dimension. p_1 and p_2 must be chosen such that $C_4^I(p_1)$ and $C_4^I(p_2)$ have opposite signs ($C_4^I(p)$ are odd functions of p, so $C_4^I(p) = -C_4^I(-p)$).

Rotary Resonance

Here, only a brief summary of the RR effects in quadrupolar nuclei is given with more extensive discussions available elsewhere [20, 24, 25]. The RR condition is satisfied when the rf amplitude, ω_1, and the rotor spinning speed, ω_r, satisfy the following condition [30, 31]:

$$\omega_1 = \frac{4n\omega_r}{2I+1}, \tag{5}$$

where n is a positive integer. At RR conditions ($\omega_1 = \frac{2}{3}n\omega_r$ for $I = \frac{5}{2}$), the CT coherence is poorly spin locked since it mixes with both the 3QC and 5QC [20, 24, 25]. MQCs are efficiently transferred to 1QC at the RR condition. The optimal rf amplitudes for MQC excitation from equilibrium magnetization (I_Z) lie between RR conditions

$$\frac{4(n-1)\omega_r}{2I+1} < \omega_1 < \frac{4n\omega_r}{2I+1}. \tag{6}$$

The optimal rf amplitudes for conversions between MQCs (e.g. 5QC to 3QC) also occur away from the RR conditions, because leakage from 3QC to 1QC is suppressed.

The second-order quadrupolar interaction causes an additional dephasing of the coherences. Additional efficiency extrema are present due to recoupling of the second-order quadrupolar terms [25]. The dephasing caused by second-order broadening results not only in shorter optimal pulse widths, but also in reduced excitation and conversion efficiencies, especially at low-rf amplitudes.

MATERIALS AND METHODS

Experimental

A sample of aluminum acetylacetonate (Aldrich, 99%, used without further purification) was ground using a mortar and pestle before it was packed into a zirconia rotor. All experiments were performed on a Chemagnetics/Varian CMX Infinity 500 spectrometer equipped with a 3.2 mm Chemagnetics MAS probe. A 20 kHz spinning speed was used for all experiments. The ^{27}A1 NMR spectra were obtained at a Larmor frequency of 130.3 MHz.

The 2D maps of MQ excitation and conversion efficiencies were collected using variation of the split-t_1 MQMAS experiment [35], where the rf amplitude and pulse width for one of the MQ excitation or conversion pulses were varied, and the other MQ excitation and/or conversion pulses were hard (150 kHz). Figure 1 depicts the two versions of the 5Q3Q mixed multiple-quantum experiment used for the 2D spectra of aluminum acetylacetonate. ($MQNQ$ notation is used to denote the two coherences used to refocus the second-order quadrupolar interaction.) One implementation used hard rf pulses (HPs), and the other used LAPs for 5QC excitation and for 5QC to 3QC conversion. In both the HP and LAP versions of the

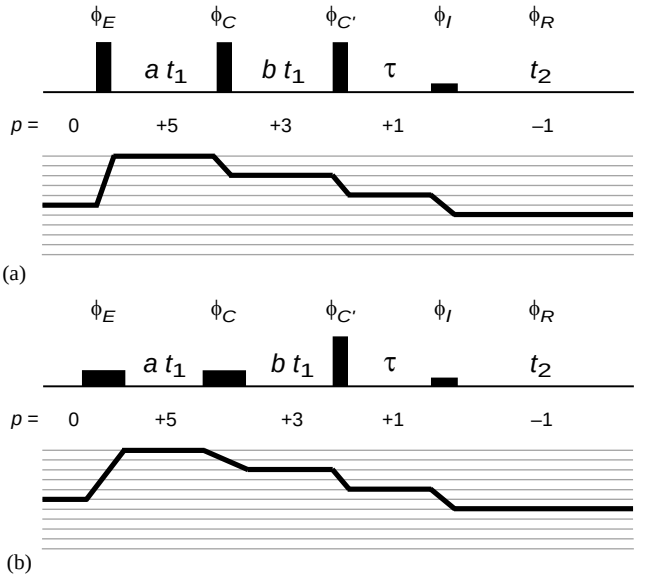

FIG. 1. Schematic of and coherence pathway diagram for the split-t_1 5Q3Q MAS experiments for $I = 5/2$ nuclei used to collect the data in Fig. 3. The evolution time in t_1 was split using $a = 19/44$ and $b = 25/44$. (a) The HP version and (b) the LAP version of the 5Q3Q experiment.

experiment, a HP was used for the 3QC to 1QC conversion, and a soft rf pulse was used to invert the CT coherence from a +1 coherence to a −1 coherence for detection. The pulse sequences and desired coherence pathways are shown in Fig. 1. The data in Fig. 2 (right column) were acquired using the 5Q1Q (Figs. 2b and 2f), 5Q3Q (Fig. 2d), and 3Q1Q (Fig. 2h) split-t_1 experiments. The a and b fractions for t_1 evolution are 3Q1Q: $a = 12/31$, $b = 19/31$; 5Q1Q: $a = 12/37$, $b = 25/37$; and 5Q3Q: $a = 19/44$, $b = 25/44$. Note that in the 3Q1Q experiment (for $I = 5/2$), the second part of t_1 comes after the soft inversion pulse.

The phase cycles for the three different $MQNQ$ experiments for $I = 5/2$ nuclei are listed in Table 1 and were checked with the CCCP program [36]. The amplitudes of the hard rf pulses were 150 kHz for all experiments, and the soft inversion pulse amplitude was 3.7 kHz. The rf amplitudes were calibrated using a 1 M $AlCl_3$(aq) sample. The pulse widths were empirically optimized to give maximum signal (details are given in the caption of Fig. 3).

Simulations

The rf, isotropic CS, and first- and second-order quadrupolar interactions were included in the simulations. A frequency offset was included to compensate for the second-order quadrupolar isotropic shift in order to set the rf pulse on-resonance. The quadrupolar parameters used in the simulations were those for aluminum acetylacetonate, $C_Q = 3.0$ MHz and $\eta = 0.15$ [37]. Simulations were performed by numerically propagating the density matrix with a 0.1 μs (1/500 of a rotor period)

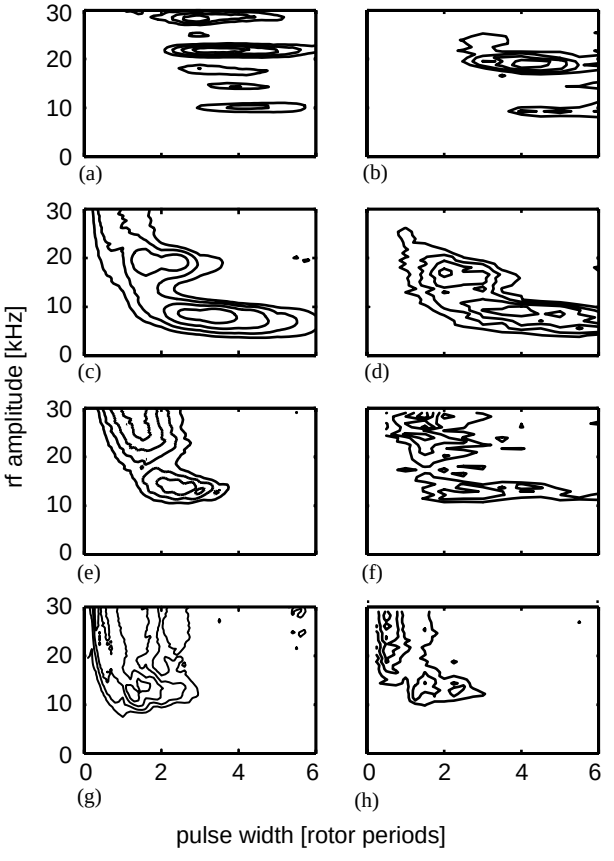

FIG. 2. 2D efficiency maps for the various MQC excitation and conversions as a function of rf amplitude and pulse width. Simulations are shown in the left column, and experimental data are shown in the right column. The efficiencies plotted for the simulations are the magnitude of density matrix element for the desired final coherence. The efficiencies plotted for the experimental data were determined by taking the maximum value of the magnitude spectrum for the first transient of the split-t_1 experiment. The rf amplitude step size is about 750 Hz for the experimental data and about 500 Hz for the simulations. The pulse width step size was 1/4 rotor period in (b), (f), and (h); 1/2 rotor period in (d); and 1/10 rotor period in (a), (c), (e), and (g). Each experimental data set was collected with one complete phase cycle for each rf amplitude and pulse width combination. The RR conditions for this spinning speed are $\omega_1 = n13.33$ kHz. The maximum percent efficiency for each excitation or conversion is given in brackets (as determined from the simulations). (a), (b) I_Z to 5QC excitation [42%]; (c), (d) 5QC to 3QC conversion [32%]; (e), (f) 5QC to 1QC conversion [14%]; and (g), (h) 3QC to 1QC conversion [23%]. Each plot has four contours at 45%, 60%, 75%, and 90% of the maximum in each map.

maximum time step between Hamiltonian evaluations. A 20 kHz spinning speed was used. Powder averaging was performed by summing the results from 3722 different crystallite orientations generated using the ZCW sampling scheme [38–40]. A Larmor frequency of 130 MHz was used for a spin $I = 5/2$ nucleus.

TABLE 1
Phase Cycles for the 3Q1Q, 5Q1Q, and 5Q3Q Experiments

Experiment	Phases	Phase list
3Q1Q	ϕ_E	$(0, 30, 60, 90, 120, 150, 180, 210, 240, 270, 300, 330)_8$
	ϕ_C	$(0)_{96}$
	ϕ_I	$(0)_{12}, (45)_{12}, (90)_{12}, (135)_{12}, (180)_{12}, (225)_{12}, (270)_{12}, (315)_{12}$
	ϕ_R	$[(0, 270, 180, 90)_3, (90, 0, 270, 180)_3, (180, 90, 0, 270)_3, (270, 180, 90, 0)_3]_2$
5Q1Q	ϕ_E	$(0, 18, 36, 54, 72, 90, 108, 126, 144, 162, 180, 198, 216, 234, 252, 270, 288, 306, 324, 342)_8$
	ϕ_C	$(0)_{160}$
	ϕ_I	$(0)_{20}, (45)_{20}, (90)_{20}, (135)_{20}, (180)_{20}, (225)_{20}, (270)_{20}, (315)_{20}$
	ϕ_R	$[(0, 270, 180, 90)_5, (90, 0, 270, 180)_5, (180, 90, 0, 270)_5, (270, 180, 90, 0)_5]_2$
5Q3Q	ϕ_E	$(0, 18, 36, 54, 72, 90, 108, 126, 144, 162, 180, 198, 216, 234, 252, 270, 288, 306, 324, 342)_{32}$
	ϕ_C	$[(0)_{20}, (90)_{20}, (180)_{20}, (270)_{20}]_8$
	$\phi_{C'}$	$(0)_{80}, (45)_{80}, (90)_{80}, (135)_{80}, (180)_{80}, (225)_{80}, (270)_{80}, (315)_{80}$
	ϕ_I	$(0)_{640}$
	ϕ_R	$\{[(0, 270, 180, 90)_5, (180, 90, 0, 270)_5]_2, [(90, 0, 270, 180)_5, (270, 180, 90, 0)_5]_2,$ $[(180, 90, 0, 270)_5, (0, 270, 180, 90)_5]_2, [(270, 180, 90, 0)_5, (90, 0, 270, 180)_5]_2\}_2$

Note. The labels ϕ_x denote the phase of the pulse or receiver. The phases are given in degrees. Subscripts indicate the number of repetitions of the phase cycle in the parentheses, brackets, or braces. There are 96, 160, and 640 steps in the 3Q1Q, 5Q1Q, and 5Q3Q phase cycles, respectively.

The simulations in Fig. 2 (left column) were made by collecting one point after a rf pulse that was varied in amplitude and width. The rf pulse width step size was 5 μs and covered the range of 5–300 μs (6 rotor periods). The rf amplitude was varied in steps of $\approx$ 500 Hz from $\approx$ 0.5 to 30 kHz (63 steps).

The simulated spectra in Fig. 4 are 1024-point FIDs collected using the detection operator I_-. The amplitude and width of each rf pulse were optimized individually for maximum coherence transfer, except for Fig. 4e, where the only difference from the conditions used for Fig. 4d was a 1 kHz larger frequency offset. The FIDs were processed by applying a 20 Hz exponential apodization, performing a discrete Fourier transformation with no zero filling, and applying a zero-order phase correction. The rf amplitudes and pulse widths are given in the caption. A filter was applied after each rf pulse that zeroed all undesired coherences in the density matrix in order to emulate a phase cycle.

RESULTS AND DISCUSSION

2D maps of the coherence transfer efficiency of rf pulses as a function of rf amplitude and pulse width are presented in Fig. 2. The left column presents simulations, and the right column presents experimental data. In all cases, the simulations are in good agreement with the experiments, with the largest difference being that the experimental rf amplitudes are shifted 1–2 kHz lower than in the numerical simulations. This difference is most likely due to the uncertainty in the rf calibration. The pulse widths of the efficiency maxima, however, match almost perfectly between the experimental data and the simulations. The contour levels

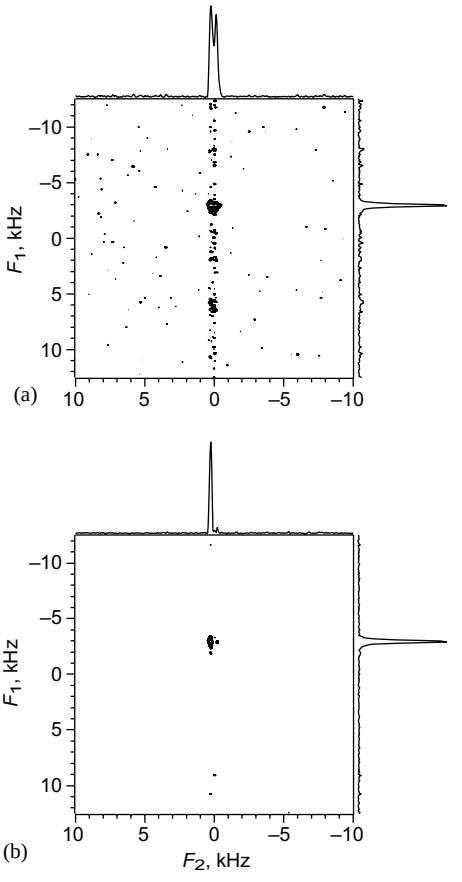

FIG. 3. Experimental spectra for the two versions of the 5Q3Q experiment, (a) HP and (b) LAP. Both the HP and LAP experiments used a 0.45 μs, 150 kHz rf pulse for the 3QC to 1QC conversion pulse and a 12.5 μs, 3.7 kHz rf pulse for the $+1$QC to -1QC inversion pulse. The dwell time was 40 μs in t_1 and 50 μs in t_2. The τ delay was 5 ms. The number of points in t_1 and t_2 were 128 and 256, respectively. The sizes of the data sets were doubled in both dimensions by zero filling prior to Fourier transformation. The HP experiment (a) used 150 kHz rf pulses of 3.4 and 0.65 μs, respectively, for 5QC excitation and 5QC to 3QC conversion; whereas the LAP experiment (b) used a 190 μs, 19 kHz 5QC excitation pulse, and a 95 μs, 6.5 kHz 5QC to 3QC pulse.

(45%, 60%, 75%, and 90% of the maximum value in each map) were placed above the noise level in the plots of the experimental data. The same contour levels were used for the simulations. For 5QC to 1QC and 3QC to 1QC conversions, there are efficiency maxima at $\omega_1 = \frac{2}{3}\omega_r$ which is a RR condition. The 5QC to 3QC conversion efficiency has minima at $\frac{2}{3}n\omega_r$, $n = 1, 2$. This drop in efficiency is due to the subsequent transfer from 3QC to 1QC. The global maximum for the 5QC excitation efficiency is in between the $n = 1$ and $n = 2$ RR conditions.

Figure 3 shows two experimental MMQMAS spectra acquired using the pulse sequences in Fig. 1. The spectrum shown in Fig. 3a was obtained using the HP

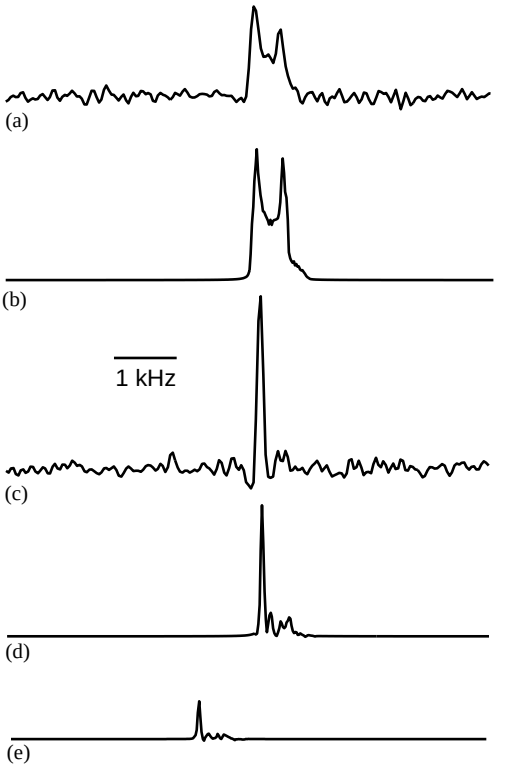

FIG. 4. Comparison of the anisotropic projections for the 5Q3Q experiment. (a) Experimental spectrum from the first transient in t_1 of the HP experiment. (b) Simulated spectrum of the F_2 projection for the HP experiment. (c) Experimental spectrum from the first transient in t_1 of the LAP experiment. (d) Simulated spectrum of the F_2 projection for the LAP experiment. (e) Simulated spectrum of the F_2 projection for an LAP experiment using the same conditions as (d), except with a 1 kHz larger frequency offset.

version of the experiment, and the spectrum shown in Fig. 3b was obtained using the LAP version of the experiment. The bottom contour is at 5% of the maximum intensity for both spectra. It is easy to see from the contours and projections that the LAP version of the experiment has a higher signal-to-noise ratio (S/N), defined here as the maximum intensity divided by the standard deviation of the noise. The S/N in the LAP experiment is twice that of the HP experiment. All possible combinations of LAPs and HPs were tried for the MQC excitation and conversion pulses. The maximum sensitivity was obtained in the experiment that used LAPs for the 5QC excitation and 5QC to 3QC conversion, and a HPs for 3QC to 1QC conversion.

Although the LAP version of the 5Q3Q experiment has a superior S/N, the anisotropic projection has a much narrower frequency distribution than the normal MAS line shape. Figures 4a and 4c show the experimental spectra for the first transient in t_1 for both the HP and LAP experiments, respectively; Figs. 4b and 4d

show the corresponding simulated spectra. The distorted line shape observed in Fig. 4c is reproduced in the simulation. The experimental spectra in Figs. 4a and 4c have the same vertical scaling, whereas the simulations in Figs. 4b and 4d have been vertically scaled such that the spectra are the same height. The simulations in Figs. 4d and 4e have the same vertical scaling to show the effects of the resonance offset on the spectral intensity. The difference in phasing between Figs. 4c and 4d is likely due to differences in the acquisition and processing. The experimental spectrum is the first transient in t_1 of a split-t_1 experiment, where an echo is acquired. In the simulations, the τ delay was omitted, and no first-order phase correction was applied.

Simply acquiring the first transient in t_1 of a split-t_1 MQMAS experiment with LAPs may be sufficient to resolve the resonances (albeit with a distorted, yet narrower, frequency distribution) for sites with low quadrupolar asymmetry. This 1D experiment precludes the determinations of the quadrupolar parameters from the full anisotropic line shape. However, in some instances (e.g. determining the number of sites present in a sample or following the shift of a resonance during the course of a reaction), when the quadrupolar parameters are not needed, a short 1D experiment is preferred over a longer 2D experiment.

A normal MAS powder pattern results from the uniform excitation of all crystallite orientations. For the case where there is no asymmetry ($\eta = 0$), the distorted anisotropic (F_2) projection in the LAP experiment is due to the fact that the LAPs are selective to crystallite orientations in two bimodal bands. One band has the powder angle β between $\beta = 35^\circ$ and 62°, with the maxima at $\beta = 40^\circ$ and 57°. The second band is at the complementary angles to the first band; between $\beta = 118^\circ$ and 145°, with the maxima at $\beta = 123^\circ$ and 140°. These bands were determined via numerical simulations.

This orientation selection mechanism breaks down as η increases. Both experiments and simulations indicate the 5QC excitation is more selective (for small η) than the 5QC to 3QC transfer. This selectivity can be reproduced in simulations without including the second-order quadrupolar Hamiltonian during the rf pulses. It should be noted that Vosegaard *et al.* [17] did not observe such radical line shape distortions in their experiments on $I = 3/2$ nuclei.

One drawback of running this 1D experiment instead of a normal, hard pulse MQMAS experiment (aside from the fact that the anisotropic information is lost) is that the coherence transfer efficiencies of the LAPs are sensitive to resonance offset effects. Figure 4e shows a simulated spectrum with conditions identical to those for Fig. 4d, except the resonance offset was 1 kHz larger. The intensity of the off-resonance spectrum (Fig. 4e) is about one quarter that of the on-resonance spectrum (Fig. 4d). Consequently, the 1D experiment, in this form, would not be quantitative. Simulations show that the efficiency of the 5QC excitation is more sensitive to resonance offsets than is the efficiency of the 5QC to 3QC conversion.

CONCLUSION

We have presented simulations detailing the rotary resonance (RR) effects in all of the high quantum transitions in $I = 5/2$ nuclei that are applicable to MQMAS and

MMQMAS experiments. Using appropriately chosen low-amplitude rf pulses (LAP) for the 5QC excitation and 5QC to 3QC conversion pulses yields an increase in the S/N by a factor of two over the hard pulse version of the 5Q3Q MMQMAS experiment. In the LAP version of the experiment, the anisotropic projection of the 5Q3Q spectrum is severely distorted when compared to the normal MAS line shape. This distortion is due to the fact that the LAPs are selective for sites with low asymmetry towards two bimodal ranges of crystallite orientations between $\beta = 35^\circ$ and 62°, and their complementary angles. When the quadrupolar asymmetry parameter is small, judicious choice of the LAP conditions may allow a spectrum with good sensitivity and sufficiently resolved resonances to be acquired in a 1D experiment, instead of using the indirect dimension projection of a 2D MQMAS experiment. However, in this case, the lack of a full powder pattern precludes obtaining the quadrupolar parameters via numerical fitting of the anisotropic line shape. In addition, this method is not quantitative since the intensities of the lines are sensitive to resonance offsets.

ACKNOWLEDGMENTS

This work was supported by the Director, Office of Science, Office of Basic Energy Sciences, Materials Sciences Division, of the US Department of Energy under Contract DE-AC03-76SF00098. A. J. thanks the Austrian Science Fund for an Erwin Schrödinger Fellowship.

REFERENCES

1. A. Abragam, "Principles of Nuclear Magnetism," Oxford Univ. Press, Oxford, 1961.
2. P. J. Bray, Nuclear magnetic-resonance studies of glass structure, *J. Non-Cryst. Solids* **73**, 19–45 (1985).
3. P. J. Grandinetti, J. H. Baltisberger, I. Farnan, J. F. Stebbins, U. Werner, and A. Pines, Solid-state ^{17}O magic-angle and dynamic-angle spinning NMR study of the SiO_2 polymorph coesite, *J. Phys. Chem.* **99**, 12341–12348 (1995).
4. J. F. Stebbins, P. Zhao, and S. Kroeker, Non-bridging oxygens in borate glasses: Characterization by ^{11}B and ^{17}O MAS and 3QMAS NMR, *Solid State Nucl. Magn. Reson.* **16**, 9–19 (2000).
5. F. Angeli, T. Charpentier, J. M. Delaye, J. C. Petit, D. Ghaleb, and P. Faucon, Influence of glass composition on the Na–O bond distance: A Na-23 3Q-MAS NMR and molecular dynamics study, *J. Non-Cryst. Solids* **276**, 132–144 (2000).
6. L. Frydman and J. S. Harwood, Isotropic spectra of half-integer quadrupolar spins from bidimensional magic-angle spinning NMR, *J. Am. Chem. Soc.* **117**, 5367–5368 (1995).
7. A. Medek, J. S. Harwood, and L. Frydman, Multiple-quantum magic-angle spinning NMR: A new method for the study of quadrupolar spins in a solid, *J. Am. Chem. Soc.* **117**, 12779–12787 (1995).
8. G. Wu, D. Rovnyak, and R. G. Griffin, Quantitative multiple-quantum magic-angle-spinning NMR spectroscopy of quadrupolar nuclei in solids, *J. Am. Chem. Soc.* **118**, 9326–9332 (1996).
9. T. Mildner, M. E. Smith, and R. Dupree, Rotationally induced triple quantum coherence excitation in MAS NMR spectroscopy of $I = 5/2$ spins, *Chem. Phys. Lett.* **301**, 389–394 (1999).
10. T. Mildner, M. E. Smith, and R. Dupree, 2D five quantum MAS NMR using rotationally induced coherence transfer, *Chem. Phys. Lett.* **306**, 297–302 (1999).
11. A. P. M. Kentgens and R. Verhagen, Advantages of double frequency sweeps in static, MAS and MQMAS NMR of spin $I = 3/2$ nuclei, *Chem. Phys. Lett.* **300**, 435–443 (1999).

12. P. K. Madhu, A. Goldbourt, L. Frydman, and S. Vega, Sensitivity enhancement of the MQMAS NMR experiment by fast amplitude modulation of the pulses, *Chem. Phys. Lett.* **307**, 41–47 (1999).
13. P. K. Madhu, A. Goldbourt, L. Frydman, and S. Vega, Fast radio-frequency amplitude modulation in multiple-quantum magic-angle-spinning nuclear magnetic resonance: Theory and experiments, *J. Chem. Phys.* **112**, 2377–2391 (2000).
14. A. Goldbourt, P. K. Madhu, and S. Vega, Enhanced conversion of triple to single-quantum coherence in the triple-quantum MAS NMR spectroscopy of spin-5/2 nuclei, *Chem. Phys. Lett.* **320**, 448–456 (2000).
15. T. Vosegaard, D. Massiot, and P. J. Grandinetti, Sensitivity enhancements in MQMAS NMR of spin-5/2 nuclei using modulated rf mixing pulses, *Chem. Phys. Lett.* **326**, 454–460 (2000).
16. Z. Yao, H.-T. Kwak, D. Sakellariou, L. Emsley, and P. J. Grandinetti, Sensitivity enhancement of the central transition NMR signal of quadrupolar nuclei under magic-angle spinning, *Chem. Phys. Lett.* **327**, 85–90 (2000).
17. T. Vosegaard, P. Florian, D. Massiot, and P. J. Grandinetti, Multiple quantum magic-angle spinning using rotary resonance excitation, *J. Chem. Phys.* **114**, 4618–4624 (2001).
18. K. H. Lim, T. Charpentier, and A. Pines, Efficient triple-quantum excitation in modified RIACT MQMAS NMR for $I = 3/2$ nuclei, *J. Magn. Reson.* **154**, 196–204 (2002).
19. P. K. Madhu and M. H. Levitt, Signal enhancement in the triple-quantum magic-angle spinning NMR of spins-$\frac{3}{2}$ in solids: The FAM-RIACT-FAM sequence, *J. Magn. Reson.* **155**, 150–155 (2002).
20. J. D. Walls, K. H. Lim, and Alexander Pines, Theoretical studies of the spin dynamics of quadrupolar nuclei at rotational resonance conditions, *J. Chem. Phys.* **116**, 79–90 (2002).
21. J. H. Shirley, Solution of the Schrödinger equation with a Hamiltonian periodic in time, *Phys. Rev.* **138**, 979–987 (1965).
22. E. Vinogradov, P. K. Madhu, and S. Vega, A bimodal Floquet analysis of phase modulated Lee–Goldburg high resolution proton magic angle spinning NMR experiments, *Chem. Phys. Lett.* **329**, 207–214 (2000).
23. E. Vinogradov, P. K. Madhu, and S. Vega, Phase modulated Lee–Goldburg magic angle spinning proton nuclear magnetic resonance experiments in the solid state: A bimodal Floquet theoretical treatment, *J. Chem. Phys.* **115**, 8983–9000 (2001).
24. Z. Gan and P. Grandinetti, Rotary resonance in multiple-quantum magic angle spinning, *Chem. Phys. Lett.* **352**, 252–261 (2002).
25. J. D. Walls, K. H. Lim, J. W. Logan, J. T. Urban, A. Jerschow, and A. Pines, Theoretical investigations of $I = 5/2$ quadrupolar spin dynamics in the sudden-passage regime, *J. Chem. Phys.* **117**, 518–532 (2002).
26. A. E. Bennett, R. G. Griffin, and S. Vega, Recoupling of homo- and heteronuclear dipolar interactions in rotating solids, *in* "NMR Basic Principles and Progress" (B. Blümich, Ed.), Vol. 33, pp. 1–78, Springer-Verlag, Berlin, 1994.
27. Z. Gan, D. M. Grant, and R. R. Ernst, NMR chemical shift anisotropy measurements by RF driven rotary resonance, *Chem. Phys. Lett.* **254**, 349–357 (1996).
28. S. Dusold and A. Sebald, Dipolar recoupling under magic-angle spinning conditions, *Annu. Rep. NMR Spectrosc.* **41**, 185–264 (2000).
29. M. Ernst, A. Samoson, and B. H. Meier, Low-power decoupling in fast magic-angle spinning NMR, *Chem. Phys. Lett.* **348**, 293–302 (2001).
30. W. Sun, J. T. Stephen, L. D. Potter, and Y. Wu, Rotation-induced resonance and second-order quadrupolar effects on spin locking of half-integer quadrupolar nuclei, *J. Magn. Reson. A* **116**, 181–188 (1995).
31. S. M. DePaul, M. Ernst, J. S. Shore, J. F. Stebbins, and A. Pines, Cross-polarization from quadrupolar nuclei to silicon using low-radio-frequency amplitudes during magic-angle spinning, *J. Phys. Chem. B* **101**, 3240–3249 (1997).
32. A. J. Vega, MAS NMR spin locking of half-integer quadrupolar nuclei, *J. Magn. Reson.* **96**, 50–68 (1992).

33. A. J. Vega, CP/MAS of quadrupolar $S = 3/2$ nuclei, *Solid State Nucl. Magn. Reson.* **1**, 17–32 (1992).
34. A. Jerschow, J. W. Logan, and A. Pines, High-resolution NMR of quadrupolar nuclei using mixed multiple-quantum coherences, *J. Magn. Reson.* **149**, 268–270 (2001).
35. S. P. Brown and S. Wimperis, Two-dimensional multiple-quantum MAS NMR of quadrupolar nuclei: A comparison of methods, *J. Magn. Reson.* **128**, 42–61 (1997).
36. A. Jerschow and N. Müller, Efficient simulation of coherence transfer pathway selection by phase cycling and pulsed field gradients in NMR, *J. Magn. Reson.* **134**, 17–29 (1998).
37. S. E. Ashbrook, S. P. Brown, and S. Wimperis, Multiple-quantum cross-polarization in MAS NMR of quadrupolar nuclei, *Chem. Phys. Lett.* **288**, 509–517 (1998).
38. S. K. Zaremba, Good lattice points, discrepancy, and numerical integration, *Ann. Mat. Pura. Appl.* **4:73**, 293–317 (1966).
39. H. Conroy, Molecular Schrödinger equation. VIII. A new method for the evaluation of multidimensional integrals, *J. Chem. Phys.* **47**, 5307–5318 (1967).
40. V. B. Cheng, H. H. Suzukawa Jr., and M. Wolfsberg, Investigations of a nonrandom numerical method for multidimensional integration, *J. Chem. Phys.* **59**, 3992–3999 (1973).